ELSEVIER

Journal of Photochemistry and Photobiology A: Chemistry 129 (1999) 89–99

Journal of Photochemistry and Photobiology A:Chemistry

www.elsevier.nl/locate/jphotochem

Photocatalytic properties of ZrO_2 and Fe/ZrO_2 semiconductors prepared by a sol–gel technique

Silvia G. Botta [a], José A. Navío [b], María C. Hidalgo [b], Gloria M. Restrepo [b], Marta I. Litter [a,*]

[a] *Unidad de Actividad Química, Comisión Nacional de Energía Atómica, Centro Atómico Constituyentes, Av. Gral. Paz 1499, (1650) San Martín, Prov. de Buenos Aires, Argentina*

[b] *Instituto de Ciencia de Materiales de Sevilla, Centro Mixto CSIC-Universidad de Sevilla, Av. Américo Vespucio, s/n, Isla de Ia Cartuja, 41092-Sevilla, Spain*

Received 5 July 1999; accepted 12 July 1999

Abstract

The photocatalytic efficiency of pure and 0.5–20 wt.% Fe-containing ZrO_2 samples, prepared by a sol–gel technique, was tested in the transformation of environmentally important substrates, such as nitrite, EDTA and Cr(VI) and compared with that of TiO_2 (Degussa P-25). All samples were active, although the efficiency was lower than that of TiO_2. Nevertheless, the presence of iron increased the activity for nitrite photooxidation, with the maximum efficiency at 5 wt.% Fe content. At higher Fe content, the efficiency decreased but it was always higher than that of the undoped sample. For EDTA oxidation and Cr(VI) reduction, the same trend was observed. Remarkably, Cr(VI) reduction in the presence of EDTA was strongly accelerated, all zirconia samples being as active as P-25, although initial rates were lower and somewhat detrimentally affected by the presence of iron. The photocatalytic activity depends on the structural, surface and optical properties of the sample, on the preparation conditions and on the nature of the photocatalytic reaction.

Keywords: Heterogeneous photocatalysis; Zirconia; Titania; Nitrite; EDTA; Cr(VI)

1. Introduction

Zirconium dioxide (ZrO_2) is an important material widely used in ceramics technology [1] and in heterogeneous catalysis [2,3]. Due to its nature as n-type semiconductor, it has been considered recently as a photocatalyst in photochemical heterogeneous reactions. The reported values of the energy of the bandgap (E_g) of this oxide range between 3.25 and 5.1 eV [4–12], depending on the preparation technique of the sample. From these, the most frequent and accepted value is 5.0 eV, with a conduction band potential of −1.0 V vs. NHE at pH 0 [13]. Accordingly, the corresponding value of the valence band potential is +4.0 V vs. NHE. The relatively wide E_g value and the high negative value of the conduction band potential allowed its use as a photocatalyst in the production of hydrogen through water decomposition [10,13,14]. Other photocatalytic reactions performed with zirconia were the oxidation of 2-propanol to acetone [12,15], the oxidation of propene [4,16] and ethane [9], the photodegradation of 4-chlorophenol [17], 4-nitrophenol [18] and 1,4-pentanediol [19], the oxidation of CO [9,20] and the reduction of HCO_3^- to CO [13,14]. Also, it was found that ZrO_2 can photocatalyze the oxygen isotopic exchange [9,21]. Kohno et al. used ZrO_2 to photocatalytically reduce CO_2 with hydrogen [22,23] and with methane [24]. In photooxidative reactions, the activity of ZrO_2 samples is generally much lower than that of TiO_2. Although ZrO_2 presents an absorption maximum around 250 nm, some samples show a non-negligible absorption in the near UV range (290–390 nm) [9,11,12,18]; moreover, some photocatalytic reactions could be performed under irradiation in this range, without the participation of light of higher energy [12,15,16,18,21,25]. Sato and Kadowaki attributed the photocatalytic activity of the ZrO_2 sample used in their work to an absorption band arising of an impurity level at 320 nm [9].

It is well known that some dopants included in a semiconductor matrix, such as Fe(III), inhibit the recombination of e^-/h^+ pairs, enhancing the photocatalytic efficiency of the processes, an effect sensitive to the amount of dopant [25]. Although the systems $Fe\text{-}O/TiO_2$ have been object of studies

* Corresponding author
E-mail address: litter@cnea.gov.ar (M.I. Litter)

1010-6030/99/$ – see front matter
PII: S1010-6030(99)00150-1

Table 1
Properties of the oxide samples

Sample Sample	Fe (wt.%)	Digestion time (h)	Calcination temperature (°C)	Calcination time (h)	S_{BET} ($m^2\ g^{-1}$)	Crystal phases	IEP	Particle size[a] (μm)	E_g[b] (eV)
0–500	0	0.5	500	24	30	monoclinic tetragonal (tr.)	5.3	5 to 50	3.7
0–600	0	3	600	3	8	monoclinic tetragonal (tr.)	ND[c]	5 to 80	3.8
0.5–500	0.5	0.5	500	24	15	monoclinic (0.7) tetragonal (0.3)	ND[c]	5 to 50	3.1
5–500	5	0.5	500	24	15	tetragonal	5.3	5 to 50	2.4
5–600	5	3	600	3	22	tetragonal	ND[c]	l0 to 200	2.3
10–500	10	3	500	24	47	tetragonal	ND[c]	5 to 90	2.3
20–500	20	3	500	24	56	tetragonal	ND[c]	5 to 60	2.2

[a] Determined by SEM.
[b] Determined from the diffuse reflectance spectra.
[c] ND = Not determined.

in the field of the heterogeneous photocatalysis [26–34], the photocatalytic properties of the Fe-O/ZrO_2 systems have been not described.

Nitrite is a common pollutant in the environment, and the oxidation to NO_3^- can take place photocatalytically in the troposphere by the action of semiconductor particles suspended in cloud water. In this way, nitrite can be one of the species responsible for the acid rain problem. Some results on the heterogeneous photocatalytic oxidation of nitrite using different semiconductors, especially TiO_2, are reported in the literature (see Refs. [28,31,32] and references therein). Chromium(VI) is also a common contaminant in industrial wastewaters coming from electroplating, leather tanning or paint-making; it is toxic, carcinogenic and has been regulated in many countries. Remediation of this pollutant consists generally in its transformation to the less harmful Cr(III), which can be eliminated then by precipitation in neutral or alkaline solutions. The photocatalytic reduction of Cr(VI) with semiconductors such as TiO_2, ZnO, CdS, ZnS and WO_3 has been widely studied (see Refs. [31,32,34,35] and references therein). EDTA is a common pollutant coming from industrial and domestic wastes, extensively used in detergents, fertilizers, herbicides, etc. Due to its effectiveness as a metallic complexant, it takes part in decontaminating and cleaning mixtures of boilers and components of nuclear reactors. As EDTA is not easily biodegradable or degradable by chlorine, its elimination has been attempted using activated carbon filters, ozonization and UV/H_2O_2, with variable results (see Ref. [34] and references therein). The photocatalytic degradation of EDTA has been tested by us with TiO_2 and Fe-doped TiO_2 samples [26,29,30,32,34]. Generally, the presence of a donor accelerates the heterogeneous photocatalytic reduction of Cr(VI), as previously reported by us and other authors (see Refs. [34] and [35] and references therein).

In a previous work, some ZrO_2-based samples, pure and doped with Fe(III), have been prepared by a sol–gel technique, and results of the structural, morphological and surface characterization as well as some spectroscopic and adsorption properties of these specimens have been presented [36–38]. In this work, photocatalytic experiments using these samples were performed in the oxidative and reductive systems mentioned above, and the relationship between the activity of the samples and their physicochemical properties were compared.

2. Experimental

2.1. Chemicals

ZrO_2 and Fe/ZrO_2 samples (named hereafter "*X*-*Y*", where *X* is the weight percentage of iron in the ZrO_2 matrix and *Y* is the calcination temperature in °C) were prepared by hydrolysis of aqueous suspensions of commercial $ZrOCl_2{\cdot}8H_2O$ (Merck) containing different amounts of $Fe(NO_3)_3{\cdot}8H_2O$ (Panreac). Aqueous ammonia (Merck, 25 wt.%) was added dropwise to the mixture with continuous stirring at pH 9–10. Two different digestion times (30 min and 3 h) were applied to the suspensions. After gelation, the solids were filtered and repeatedly washed until negative $AgNO_3$ test, to ensure the absence of chloride ions in the samples, as confirmed by XPS analysis. The samples were dried at 100°C for 24 h and the gel precursors were annealed at several temperatures, without a heating rate. Pure ZrO_2 samples were prepared by the same procedure but in the absence of iron. TiO_2 (Degussa P-25) was a commercial sample, kindly supplied by the manufacturer (Degussa A.G., Germany) and used as provided. The main characteristics of the oxide samples are listed in Table 1, taken from Refs. [36] and [37]. More detailed information concerning the preparation and characterization of these samples will be reported hereafter [38].

$NaNO_2$ (Merck), Na_2EDTA (Carlo Erba) and $K_2Cr_2O_7$ (Carlo Erba) were of quality grade and used as provided. All other reagents were at least of reagent grade, and used without further purification. Water was double-distilled in a

quartz apparatus. Diluted $HClO_4$ and NaOH were used for pH adjustments.

2.2. Photocatalytic studies

Irradiations were performed using a high-pressure xenon arc lamp (Osram XBO, 150 W) with a bandpass filter (Schott catalog No. BG 1, thickness 3 mm; 270 nm < λ < 510 nm; maximum transmission (87%) at 360 nm). The IR fraction of the incident light was removed by a suitable filter (Schott catalog No. KG 5). Actinometric measurements were performed by the ferrioxalate method [39]. A photon flow per unit volume of 1.5×10^{-5} Einstein $dm^3\ s^{-1}$ was calculated.

UV–visible absorption measurements were performed on a Shimadzu 210A spectrophotometer.

Photocatalytic runs were done in a thermostatted cylindrical Pyrex cell. In all cases, a fresh solution (10 cm^3) of the substrate at a known concentration was adjusted to the desired pH, and the catalyst was suspended in the solution immediately before the irradiation. The concentration of all ZrO_2-based samples in the photocatalytic experiments was 4.0 g dm^{-3}. Comparative tests with 1.0 g dm^{-3} TiO_2 (P-25) were carried out. All oxide concentrations guaranteed total light absorption.

Prior to irradiation, suspensions were kept in the dark and stirred at 25°C a time enough to assure substrate-surface equilibrium. The extent of adsorption of the substrate on the catalyst was determined by measuring concentrations before and after stirring.

Irradiations for a fixed period of time were performed under magnetic stirring. Samples were periodically withdrawn and filtered through a 0.22 μm Millipore filter. At least, duplicated runs were carried out for each condition, averaging the results. In all cases, the adsorption in the dark was discounted.

Nitrite experiments were performed at 1.0 mmol dm^3 and different pH conditions. The suspensions were stirred for 45 min until equilibration; a water-saturated oxygen stream was bubbled in the suspension at a constant rate (1.4 $cm^3\ min^{-1}$) during the whole experiment. The final nitrite concentration was determined in the filtered solution by spectrophotometry at 520 nm using the sulphanilic acid method [40]. No nitrite conversion was observed in the absence of oxide.

The oxidative degradation of EDTA was performed using 1.0 mmol dm^3 suspensions at pH 2 with the reactor open to air. Suspensions were stirred in the dark for 30 min before irradiation. EDTA concentration was evaluated by spectrophotometric analysis of the Co(III) complex [41]. No reaction was observed in the absence of oxide.

In the case of Cr(VI) experiments, 0.4 mmol dm^3 $K_2Cr_2O_7$ solutions at pH 2 were used and suspensions were stirred for 30 min before irradiation. Experiments were performed with the cell open to air. Changes in Cr(VI) concentration were followed by UV spectrophotometry at 349 nm [42]. These experiments were repeated in the presence of 1.0 mmol dm^3 EDTA.

2.3. Photocorrosion of the catalyst

Fe and Zr were analyzed in the filtered solution after irradiation in order to study the photostability of the ZrO_2-based materials. Dissolved zirconium was evaluated by the alizarin method [43]. For iron-containing oxides, total iron in solution was determined by the thioglycolate method [44].

3. Results

3.1. Photocatalytic nitrite oxidation

Fig. 1 shows the time course of nitrite oxidation under irradiation using the pure 0–500 and 0–600 samples as photocatalysts. Results in the absence of light are also shown. Normalized concentration was plotted against reaction time to circumvent slight differences in concentration between experiments. All data have been corrected discounting the adsorption after 45 min stirring in the dark. Both pure zirconia samples were active; the reaction cannot be attributed to a thermal effect since in the dark the decrease in NO_2^- concentration was almost negligible after 4 h irradiation. It can be observed that the sample calcined at 600°C was slightly more active.

The effect of the thermal treatment on the photocatalytic behavior of the samples is shown in Fig. 2. As it can be

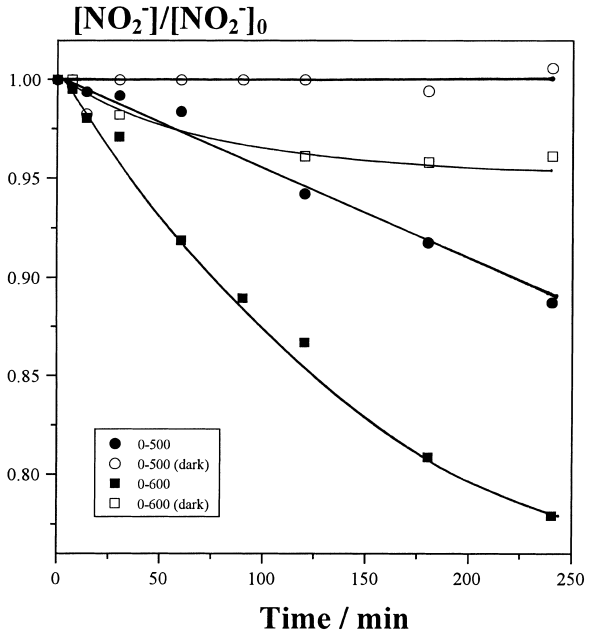

Fig. 1. Normalized concentration vs. time for NO_2^- oxidation over different oxides in the presence and absence of light. Conditions: [oxide] = 4 g dm^3; [NO_2^-] 1.0 mmol dm^3; pH 4; $T = 25$°C; $I_0 = 1.5 \times 10^5$ Einstein $dm^3\ s^{-1}$; O_2 bubbling.

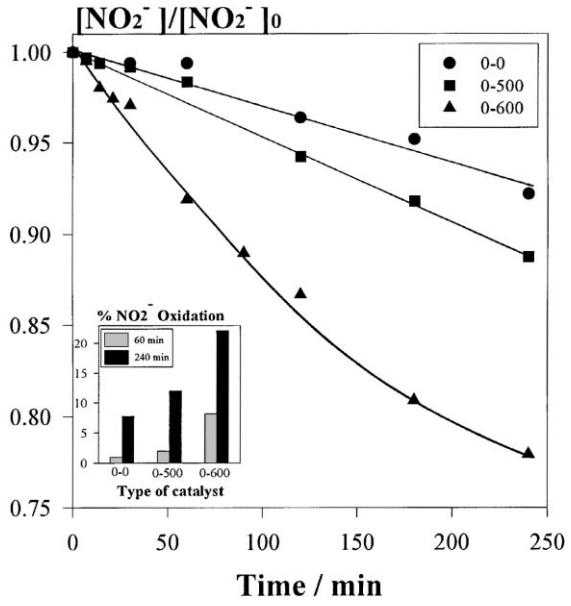

Fig. 2. Normalized concentration vs. time for NO_2^- oxidation over different ZrO_2 samples with different thermal treatments. Inset: % nitrite oxidation at two irradiation times. Same conditions as in Fig. 1.

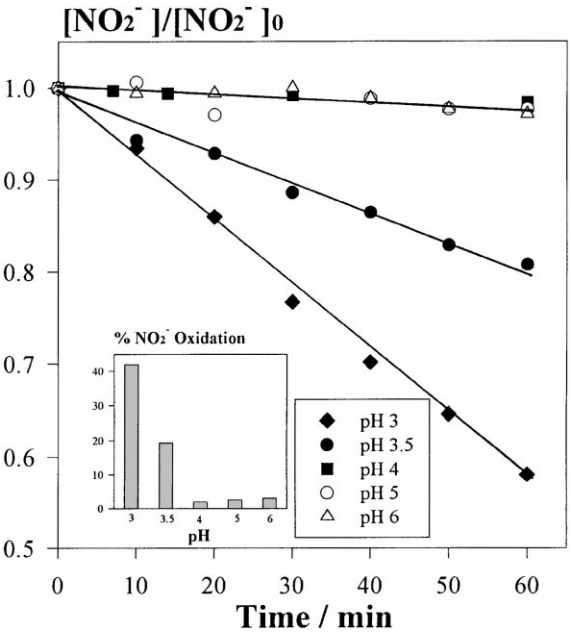

Fig. 3. Normalized concentration vs. time for NO_2^- oxidation over 0–500 at different pH. Inset: % nitrite oxidation at different pH_{in} after 60 min irradiation. Same conditions as in Fig. 1.

seen, the activity increased with the calcination temperature. Samples not calcined (0–0) or calcined at a lower temperature (0–500) gave rise to a constant reaction rate, while for the sample calcined at 600°C a slight deceleration occurred at long irradiation times (180 min).

The effect of pH was studied with pure 0–500 as the catalyst. In Fig. 3, the concentration profiles and the photooxidation degree after 1 h irradiation are presented. It can be observed that both the photocatalytic efficiency and the reaction rate decreased as the pH of the suspension increased. From pH 4 and up, the reaction rate was almost similar. Decelerating effects in concentration profiles were not observed, at least up to 60 min irradiation.

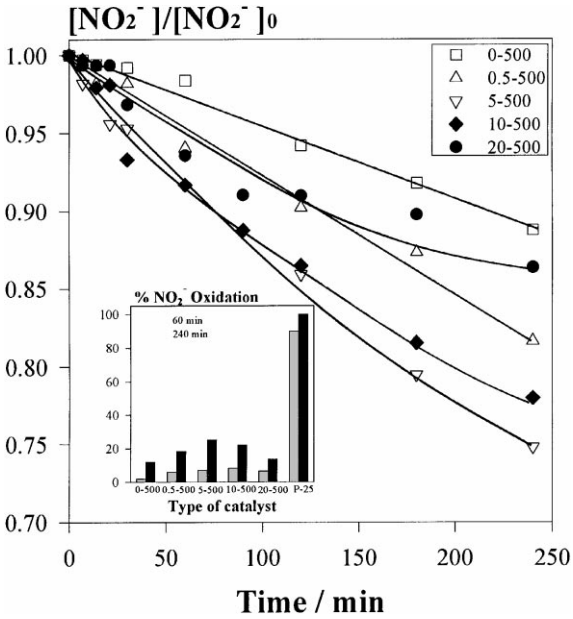

Fig. 4. Normalized concentration vs. time for NO_2^- oxidation over Fe-doped zirconia with different iron loadings. Inset: % nitrite oxidation at different pH at two irradiation times. Same conditions as in Fig. 1.

Table 2
pH_{in}, pH_{fin} and % initial (dark) adsorption of NO_2^- in the photocatalytic experiments

Photocatalyst	pH	pH_{fin}	% Initial NO_2^- adsorption
0–0	4.0 ± 0.1	5.7 ± 0.1	3.5
0–500	3.0 ± 0.1	3.3 ± 0.1	35.5
0–500	3.5 ± 0.1	4.0 ± 0.1	14.6
0–500	4.0 ± 01	5.6 ± 01	5.4
0–500	5.0 ± 0.1	5.9 ± 0.1	1.4
0–500	6.0 ± 0.1	6.3 ± 0.1	1.1
0.5–500	4.0 ± 0.1	5.0 ± 0.1	6.9
5–500	4.0 ± 0.1	4.6 ± 0.1	14.6
10–500	4.0 ± 0.1	4.6 ± 0.1	10.2
20–500	4.0 ± 0.1	4.9 ± 0.1	8.9
0–600	4.0 ± 0.1	5.5 ± 0.1	7.8
TiO_2 (P-25)	4.0 ± 0.1	6.1 ± 0.1	7.9

The effect of Fe-doping was studied by irradiating suspensions at pH 4 over zirconia samples with different iron contents (0, 0.5, 5, 10 and 20%). Fig. 4 shows the results. At low Fe content, an increase in the photocatalytic activity was observed with a maximum at 5 wt.% Fe after 240 min irradiation. For iron contents higher than 5 wt.%, the activity decreased, but it was still higher than that of the undoped sample. As expected, results over TiO_2 (P-25) show that this oxide is the most active material for this reaction. Concentration profiles as a function of time for 0–500 and 0.5–500 showed a linear kinetic behavior, while in the case of a higher Fe loading a decelerating effect was observed.

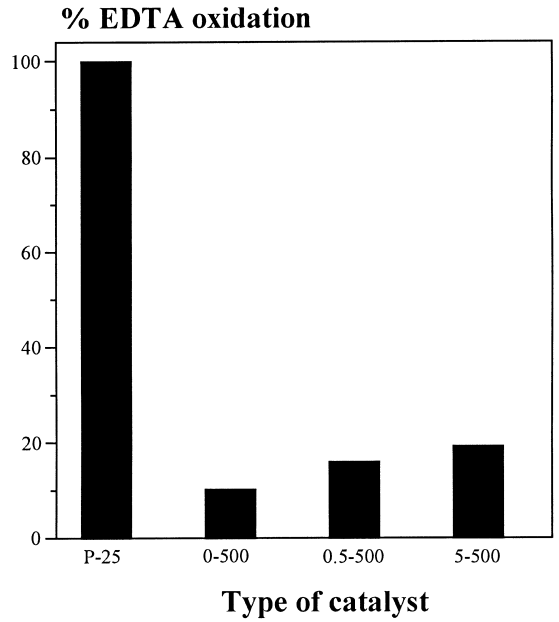

Fig. 5. Photodegradation of EDTA over different photocatalysts. Conditions: [oxide] = 4 g dm^{-3}; [TiO_2] = 1 g dm^{-3}; pH 2; irradiation time = 120 min; T = 25°C; $I_0 = 1.5 \times 10^5$ Einstein dm^{-3} s^{-1}; open to air.

Table 3
% Initial (dark) adsorption of EDTA in the photocatalytic experiments

Photocatalyst	% Initial EDTA adsorption
0–500	29.3
0.5–500	24.4
5–500	26.2
TiO_2 (P-25)	0

In Table 2, initial (pH_{in}) and final (pH_{fin}) pH values are presented as well as the adsorption of the substrate in the dark for each photocatalytic condition, taken from Refs. [36] and [38]. In all cases, an increase in pH after 240 min irradiation was observed, slightly lower at a low pH.

3.2. EDTA degradation

Fig. 5 shows the degree of EDTA degradation after 2 h irradiation over different samples (0–500, 0.5–500 and 5–500) as catalysts. For comparative purposes, a similar experiment over TiO_2 (P-25) is also shown. The photocatalytic efficiencies of all ZrO_2-based catalysts were remarkably lower than that of P-25, but the conversion degree increased slightly with the amount of iron.

No changes in pH (at pH_{in} 2) were observed after irradiation. The adsorption of the substrate in the dark is presented in Table 3, taken from Refs. [36] and [38].

3.3. Cr(VI) photocatalytic reduction

The effect of irradiation on Cr(VI) suspensions at pH 2 containing different photocatalysts (0–500, 5–500 and TiO_2 P-25) is shown in Fig. 6. ZrO_2-based samples presented a very low photocatalytic activity compared with that of P-25; however, the efficiency increased with Fe-doping as it was observed in the previous cases.

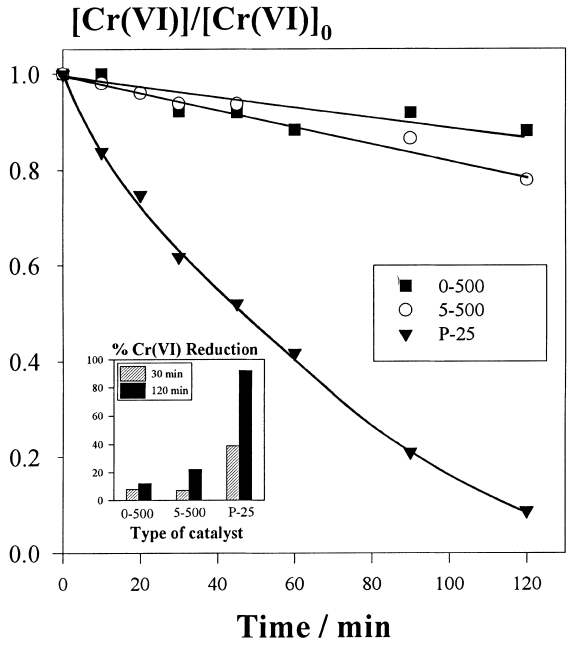

Fig. 6. Normalized concentration vs. time for Cr(VI) reduction over different catalysts. Inset: % Cr(VI) reduction at two irradiation times. Conditions: [oxide] = 4 g dm^{-3}; [TiO_2] = 1 g dm^{-3}; [Cr(VI)] = 0.4 mmol dm^{-3}; pH 2; T = 25°C; $I_0 = 1.5 \times 10^{-5}$ Einstein dm^{-3} s^{-1}; open to air.

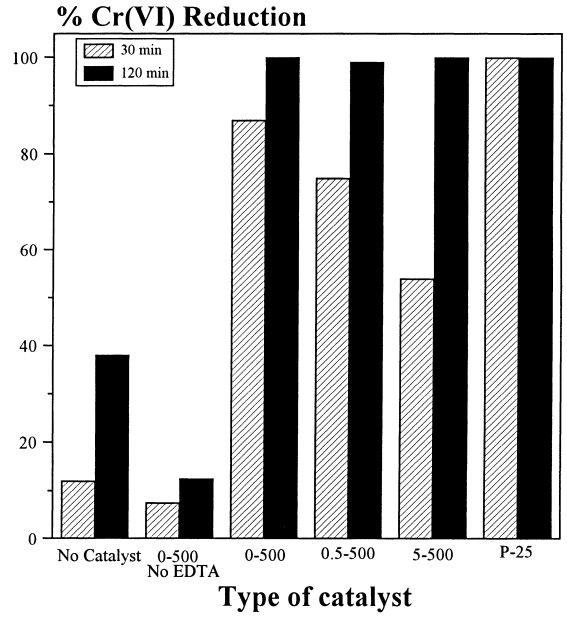

Fig. 7. % Cr(VI) reduction at two irradiation times in the presence of EDTA over different catalysts. [EDTA] = 1.0 mmol dm^{-3}. Same conditions as in Fig. 6.

The degree of Cr(VI) photocatalytic reduction after 30 and 120 min over different photocatalysts in the presence of 1.0 mmol dm^3 EDTA is presented in Fig. 7. For comparative

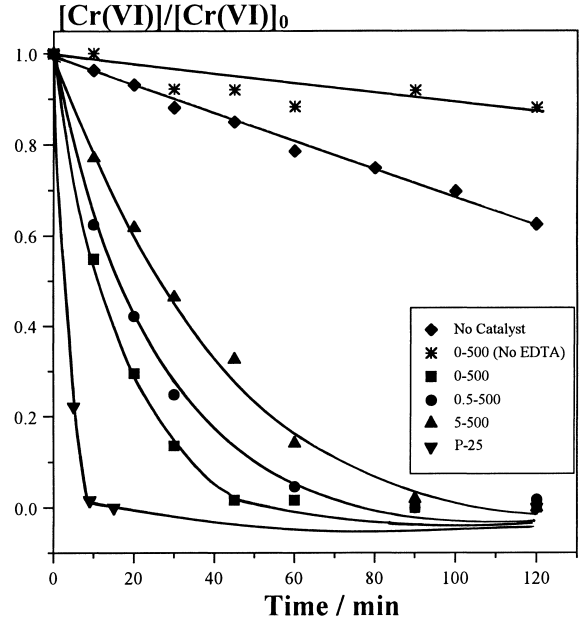

Fig. 8. Normalized concentration vs. time for Cr(VI) reduction(VI) in the presence of EDTA over different catalysts. Same conditions as in Fig. 6.

Table 4
% Cr(VI) initial (dark) adsorption in the different experiments

Photocatalyst	% Initial Cr(VI) adsorption (without EDTA)	% Initial Cr(VI) adsorption (with EDTA)
0–500	40.5	20.4
0.5–500	ND[a]	27.7
5–500	44.4	30.4
TiO_2 (P-25)	13.6	17.1

[a] ND = Not determined.

purposes, the results in the absence of photocatalyst and over 0–500 in the absence of EDTA are included. It can be observed that the extent of Cr(VI) reduction with EDTA under irradiation in the absence of catalyst, i.e. the homogeneous photochemical reaction, is significant. The same reaction in the dark was negligible (at least up to 2 h). After 120 min irradiation, all oxides presented a similar photocatalytic efficiency, comparable with that of P-25. However, after shorter irradiation times, a deleterious effect of Fe-doping on the photocatalytic activity could be observed. Concentration profiles show a dramatic acceleration of the Cr(VI) reduction by addition of EDTA, with a slower initial rate in the most loaded samples (cf. Figs. 6 and 8).

Either in the presence or in the absence of EDTA, no changes in pH were observed at the end of the experiment. The amount of Cr(VI) adsorbed on zirconia samples after equilibration in the dark (with and without EDTA) is presented in Table 4, and is taken from Refs. [36] and [38].

3.4. Deactivation of the catalysts

At the end of irradiation, Zr and Fe (for Fe-containing samples) were determined in the filtered solution. As neither Zr nor Fe was detected in solution, it was concluded that the samples were photostable in the present conditions.

4. Discussion

4.1. Mechanism

The heterogeneous photocatalytic process is a complex sequence of reactions that can be expressed by the following set of simplified equations:

$$SC \xrightarrow[E \geq E_g]{h\nu} e_{cb}^- + h_{vb}^+ \rightarrow \text{recombination} \quad (1)$$

$$h_{vb}^+ + H_2O_{ads} \rightarrow HO_{ads}^\bullet + H^+ \quad (2)$$

$$h_{vb}^+ + HO_{ads}^- \rightarrow HO_{ads}^\bullet \quad (3)$$

$$h_{vb}^+ + D_{ads} \rightarrow D_{ads}^+ \quad (4)$$

$$HO^\bullet + D_{ads} \rightarrow D_{oxid} \quad (5)$$

$$e_{cb}^- + A_{ads} \rightarrow A_{ads}^- \quad (6)$$

where D and A are respectively donors and acceptors.

The oxidative pathway can be performed by direct hole attack or mediated by $HO^\bullet$ radicals, in their free or adsorbed form, depending on the substrate. In many cases, complete mineralization of an organic substrate to CO_2 and H_2O occurs. Generally, "A" is dissolved O_2, which is transformed in superoxide radical anion.($O_2^{\bullet -}$) and can lead to the additional formation of $HO^\bullet$:

$$e_{cb}^- + O_{2_{ads}} \rightarrow O_2^{\bullet -} \xrightarrow{e^-} \rightarrow HO^\bullet \quad (7)$$

"A" can be also a metal ion species transformed to a different oxidation state species:

$$M^{n+} + z e_{cb}^- \rightarrow M^{(n-z)+} \quad (8)$$

4.1.1. NO_2^- oxidation

In a heterogeneous photocatalytic system, nitrite is anodically oxidized to nitrate while O_2 is reduced:

$$NO_2^- + H_2O \rightarrow NO_3^- + 2H^+ + 2e^- \quad (9)$$

$$O_2 + 4H^+ + 4e^- \rightarrow 2H_2O \quad (10)$$

The net reaction is therefore:

$$2NO_2^- + O_2 \rightarrow 2NO_3^- \quad (11)$$

In previous papers we have proposed the following mechanism for the photocatalytic oxidation of nitrite [31,32]

$$NO_2^- + HO^\bullet \rightarrow HNO_3^{\bullet -} \Leftrightarrow (NO_3^\bullet)^{2-} + H^+ \quad (12)$$

$$HNO_3^{\bullet -} \rightarrow NO_2^\bullet + OH^- \quad (13)$$

$$(NO_3^\bullet)^{2-} + H_2O \rightarrow NO_2^\bullet + 2OH^- \quad (14)$$

$$2NO_2^\bullet \rightarrow N_2O_4 \quad (15)$$

$$N_2O_4 + H_2O \rightarrow NO_3^- + NO_2^- + 2H^+ \quad (16)$$

$$NO_2^\bullet + HO^\bullet \rightarrow HO_2NO \quad (17)$$

$$HO_2NO \Leftrightarrow NO_3^- + H^+ \quad (18)$$

$$(NO_3^\bullet)^{2-} + O_2 \rightarrow NO_3^\bullet + O_2^{\bullet -} \quad (19)$$

The reductive pathway is expressed by Eq. (7), and contributes also to $HO^\bullet$ generation and nitrite oxidation. Other reactions related to the photochemistry of nitrogen species might also take place, such as the reaction of NO_2^- with e_{cb}^- (provided the redox potential of the conduction band of the ZrO_2 samples was thermodynamically enough), but they would end equally in nitrate formation [45].

4.1.2. Oxidative degradation of EDTA

In the case of EDTA, direct oxidation by holes or attack by $HO^\bullet$ produces hydrogen abstraction, leading to a carboxyl radical as the primary oxidation product:

$$RCOOH + h^+(HO^\bullet) \rightarrow RCOO^\bullet + H^+(H_2O) \rightarrow CO_2 + \text{other products} \quad (20)$$

The cathodic process is the reduction of oxygen (Eq. (7)), which contributes also to EDTA oxidation.

4.1.3. Reduction of Cr(VI)

The cathodic photocatalytic reaction in this system is the three electron-reduction of Cr(VI) to Cr(III) whereas the conjugate anodic reaction is the oxidation of water to oxygen. Successive one-electron reducing steps have been proposed [31,32,34,35], ending in Cr(III), the stable final product:

$$Cr^{VI} \xrightarrow{e^-} Cr^{V} \xrightarrow{e^-} Cr^{IV} \xrightarrow{e^-} Cr^{III} \quad (21)$$

$$\tfrac{1}{2}H_2O + h^+ \rightarrow \tfrac{1}{4}O_2 + H^+ \quad (22)$$

The net reaction at pH 2 is:

$$2Cr_2O_7^{2-} + 16H^+ \rightarrow 4Cr^{3+} + 8H_2O + 3O_2 \quad (23)$$

The oxidative pathway, i.e. oxidation of water by holes (Eq. (22)), is kinetically slow. When no hole or hydroxyl radical scavengers are present, recombination of electrons and holes is a competing reaction that lowers the efficiency of Cr(VI) reduction. In the presence of a donor such as EDTA, a cooperative action of both substrates was observed, leading to an increased rate of photocatalytic transformation ([34, 35] and references therein]).

4.2. Photocatalytic efficiency

The efficiency of a catalyst in heterogeneous photocatalytic systems under polychromatic irradiation is evaluated generally through the photonic efficiency (ξ%) [46]:

$$\xi\% = \frac{-\mathrm{d}C/\mathrm{d}t}{P_0} \times 100$$

Table 5
Calculated photonic efficiencies for the photocatalytic oxidation of nitrite in different conditions

Photocatalyst	pH_{in}	ξ%
0–0	4.0 ± 0.1	0.03
0–500	3.0 ± 0.1	0.52
0–500	3.5 ± 0.1	0.32
0–500	4.0 ± 0.1	0.05
0–500	5.0 ± 0.1	0.05
0–500	6.0 ± 0.1	0.04
0.5–500	4.0 ± 01	0.09
5–500	4.0 ± 01	0.15
10–500	4.0 ± 0.1	0.13
20–500	4.0 ± 01	0.10
0–600	4.0 ± 01	0.10
TiO_2 (P-25)	4.0 ± 0.1	2.48

where $-\mathrm{d}C/\mathrm{d}t$ is the reaction rate and P_0 is the incident photonic flow per unit volume.

The photonic efficiency allows to compare experiments performed in similar conditions of substrate and oxide concentration, geometry, incident light intensity and is only valid for each experimental condition. Photonic efficiencies calculated at initial times allow the evaluation of the true initial activity, intrinsic of each sample, and independent of any type of inactivation, inhibition or other secondary effect that could appear at long irradiation times.

4.2.1. NO_2^- oxidation

In this case, the efficiencies were calculated from initial rates (determined graphically), and are shown in Table 5. As expected, the photonic efficiency of P-25 is largely higher than that of ZrO_2-based catalysts. From values in Table 5 and the corresponding concentration profiles, the following conclusions can be withdrawn:

4.2.1.1. Calcination temperature. Photocatalysts calcined at different temperatures present differences in initial photonic efficiencies: pure ZrO_2 calcined at 500°C is 35% more efficient than the amorphous oxide, but a 100°C increase in the calcination temperature doubles the activity. This tendency is also maintained at long irradiation times (see Fig. 2). Different factors could account for these results. Regarding differences in initial substrate adsorption (see Table 2), the higher activity of the semiconductor treated at the highest temperature could be attributed to the higher adsorption. However, this adsorption cannot be correlated with the S_{BET} of the sample, since our results show a decrease in the specific surface with the increase of the calcination temperature (see Table 1). Consequently, the specific surface area does not seem to be a determining factor. The weak correlation between activity and specific surface is a common fact in heterogeneous photocatalysis [46]. In addition, the IR spectra of the samples [36–38] show that the bands of adsorbed water and adsorbed hydroxyl groups are less intense in the samples calcined at 600°C, suggesting a lower activity for these samples. However, this is not the

result of the photocatalytic experiments. The higher activity of 0–600 could be attributed then to a higher crystallinity degree resulting from the modification of the parameters during the preparation procedure (3 h of digestion time and 3 h of annealing at 600°C), reinforced by the fact that the non calcined (amorphous) sample shows the lowest activity. Without a thermal treatment or after a calcination at low temperature, crystal defects could remain in the sample, acting then as recombination centers for e^-/h^+ pairs. Besides, the calcination procedure could lead to surface changes, affecting the type of active sites. The combination of all these factors could be responsible for the differences in the activity of ZrO_2 samples prepared in slightly different conditions and calcined at different temperatures.

4.2.1.2. pH. Table 5 shows a decrease in the initial photonic efficiency of 0–500 with increasing pH, reaching a constant value from pH 4 and up. This behavior is kept at long reaction times (see Fig. 3). This effect could be attributed to a decrease in the initial nitrite adsorption as long as pH increases.

The increase in pH observed at the end of the reaction in all experiments (see Table 2) cannot be assigned to the global photochemical process (Eq. (11)), but to the different trends of the oxide samples to adsorb H^+ or OH^- depending on pH_{in}. Experiments performed in the dark showed an increase in pH after 4 h stirring, which reinforces the previous hypothesis.

4.2.1.3. Fe content. Table 5 shows that the initial photonic efficiency increases with the Fe content, attaining a maximum at 5 wt.% iron. After 240 min, these differences in relative efficiency are maintained (see Fig. 4). These results agree with those previously obtained by us regarding oxygen photoadsorption, which go from a very slight ability in the undoped sample to a more pronounced value in the case of doped samples. However, this effect is reported to be maximum for the 0.5 wt.% Fe sample [37,38].

From Table 1, it is observed that S_{BET} values increase with the Fe content and that the initial adsorption of the substrate follows the same trend until 5 wt.% (Table 2). Although both factors could lead to an increase in efficiency, this shows again that S_{BET} is not a determining factor, since 5-500 is the most efficient sample compared with more loaded samples, in spite of its lower surface. The observed variation could be thus explained by the effect of Fe(III) ions in the ZrO_2 matrix that, depending on the iron content, can be positive or negative. On one side, Fe can act as a trap of e^- or h^+

$$Fe^{3+} + e^- \rightarrow Fe^{2+} \quad (25)$$

$$Fe^{3+} + h^+ \rightarrow Fe^{4+} \quad (26)$$

If the conduction and valence band potentials of the semiconductor samples are thermodynamically favorable for both trapping processes, the presence of a doping agent would lead to a decrease in the recombination rate and to an increase in the photocatalytic efficiency [26,46]. On the other side, if the Fe content is high, it can act as a recombination site, influencing negatively the activity. It has been noticed that this is a determining effect in the case of Ti oxides doped with Fe [31].

It is worthwhile to remember that the incorporation of iron into a ZrO_2 matrix leads to a transformation of phase from monoclinic to tetragonal with a distortion of the lattice [47]; these factors can affect the substrate-surface affinity and the we of the sample and, in consequence, could modify the photocatalytic efficiency.

It should be taken into account that an increase in Fe content increases the absorption in the visible range of the semiconductor sample [36,38]. Therefore, provided that the bands in the visible range are photochemically active, a more efficient use of the incident radiation could lead to an increase of the efficiency. However, the 20–500 sample, which shows the highest absorption, is not the most active specimen. We conclude that the spectroscopic properties are not a determining factor for the photocatalytic activity. This fact has been previously observed in the case of Fe/Ti oxides [31,32,34].

In an isolated experiment, the photocatalytic activity of 5–600 for NO_2^- oxidation was tested. The efficiency of this sample was found to be lower than that of 0–600, suggesting that the effect of Fe content on zirconia depends also on the calcination temperature.

The IR spectra of the samples [36–38] do not reveal special differences concerning the hydration and hydroxylation degree of the Fe-containing samples compared with the pure specimens. Therefore, differences in activity cannot be explained by this factor.

4.2.1.4. Inhibition: possible reasons. As mentioned previously, nitrite oxidation to form nitrate is a slow process at room temperature. O_2 is essential in the photocatalytic reaction, because it acts in the conjugate reduction reaction and decreases the recombination rate. In its absence, the process is very slow. When NO_3^- produced in the reaction reaches a considerable concentration, it can compete with O_2 for the photogenerated e^- [31]:

$$NO_3^- + e^- \rightarrow (NO_3^{\bullet})^{2-} \quad (27)$$

$(NO_3^{\bullet})^{2-}$ reacts through reaction (14) yielding $NO_2^{\bullet}$, which can react with superoxide radical anion formed through reactions (7) and (19), regenerating nitrite and oxygen (reaction (28)):

$$NO_2^{\bullet} + O_2^{\bullet -} \rightarrow NO_2^- + O_2$$

This effect could decrease the photocatalytic efficiency and could explain the deceleration observed with the most active photocatalysts (5–500, 10–500 and 20–500) (see Fig. 4) and also with TiO_2 (not shown). Inhibition by competitive adsorption of NO_3^- is also possible [31].

Table 6
Calculated photonic efficiencies for Cr(VI) reduction in the absence and the presence of EDTA

Photocatalyst	ξ% (without EDTA)	ξ% (with EDTA)
No photocatalyst	ND	0.35
0–500	0.07	4.15
0.5–500	ND[a]	3.11
5–500	0.10	1.4
TiO_2 (P-25)	1.43	13.1

[a] ND = Not determined.

4.2.2. Oxidative degradation of EDTA

In this work, kinetic curves for EDTA degradation were not performed, precluding the calculation of photonic efficiencies. The evaluation of the photocatalyst efficiency was made taking into account the results obtained after 120 min of irradiation (see Fig. 5).

As in the case of nitrite oxidation, ZrO_2 samples were much less active than P-25. There is a slight increase in ZrO_2 activity with the increase on the Fe(III) content. The amount of EDTA adsorbed on the different photocatalysts was similar (Table 3); then, differences in efficiency cannot be attributed to differences in substrate adsorption.

In the case of Fe-doped TiO_2 photocatalysts, it has been suggested that photolysis (or/and photocatalysis) of surface or homogeneous complexes formed between EDTA and dissolved or surface iron, can contribute additionally to EDTA oxidation [26,34]. If the homogeneous complexes were formed also in the Fe/ZrO_2 systems, their photolysis and photocatalysis would contribute to EDTA oxidation according to reactions of the following type:

$$(>)Fe^{III}\text{–EDTA} + h\nu \rightarrow (>)Fe^{II} + \text{oxidation products of EDTA} \quad (29)$$

where '>' indicates surface species.

However, the production of Fe(III)–EDTA complexes in solution should be ruled out since no iron dissolution was observed. In addition, isoelectric point (IEP) data for (0–500) and (5–500) suggest that there is no Fe(III) excess on the oxide surface of these samples (see Table 1); moreover, XPS data indicate a lower amount of iron on the surface compared with that in the bulk [36,37]. Therefore, a significant contribution of surface complexes should be also ruled out, avoiding contribution of Fe(III)–EDTA photolytic reactions to the degradation of the organic compound.

The improvement in the photocatalytic activity by the presence of iron in the ZrO_2 matrix can be then explained, as in the NO_2^- case, by the effect of Fe(III) as a trapping center for the photogenerated charges.

4.2.3. Cr(VI) reduction

Table 6 shows initial photonic efficiencies for Cr(VI) reduction in the presence and in the absence of EDTA (initial rates calculated from Fig. 8). The profiles of Cr(VI) reduction in the presence of EDTA could be fitted by first order equations. Initial rates were calculated taking into account the apparent first order constant (initial rate = k_{app} [Cr(VI)]$_0$).

Both in the presence and in the absence of the reductant, P-25 showed the highest initial efficiency. In the absence of EDTA, ξ% increases with the Fe-loading (at least up to 5 wt.% Fe). This trend is maintained at long irradiation times (up to 120 min, see Fig. 8). The effect of iron can be explained by the increase in the substrate adsorption at higher Fe contents (see Table 4) and by the improvement of the charge trapping rate vs. charge recombination rate ratio.

When EDTA was added to the system, a large increase in the initial photonic efficiency (more than one order) was promoted. However, contrary to that observed in the previous cases, the efficiency decreased with the Fe-doping, being lower for the most loaded sample. So far, we do not have an easy interpretation of this experimental observation. In the absence of a photocatalyst, Cr(VI) reduction by EDTA (negligible in the dark) is significant. However, the addition of the semiconductor increases noticeably the efficiency, proving that it acts as a true photocatalyst. At longer irradiation times (30 min, the tendency of the decrease of the activity with the Fe content is kept (see Fig. 7). It is worthwhile to remark that after 120 min irradiation all the samples presented similar efficiencies, comparable with that of P-25, and that Cr(VI) conversion was total with all the samples.

Although the Cr(VI) adsorption in the presence of EDTA on ZrO_2-type catalysts is lower than in its absence (see Table 4), a significant increase in the photocatalytic activity is observed. An increase in the efficiency for Cr(VI) reduction in the presence of organic donors has already been observed for TiO_2 and Fe/TiO_2 ([34, 35] and references therein). As said before, EDTA is an efficient trap of h^+ or $HO^\bullet$ and, in its presence, recombination rate is surely lower. Analogously, an increase in EDTA oxidation efficiency should have been observed by the addition of Cr(VI) (not verified experimentally in this work).

The direct photolysis of Cr(VI)–EDTA complexes might be proposed as a contribution to the photocatalytic reduction of Cr(VI), but it has been suggested that the formation of these complexes is negligible [48]. However, for the Cr(V)–EDTA complex, a possible intermediate of the reaction, a rapid intramolecular electron transfer process leading to Cr(III) complexes has been postulated [49] and, therefore, their contribution to the acceleration of the photocatalytic reaction should not be discarded. In a similar study of the Cr(VI)/4-chlorophenol system, Fu et al. detected an increased absorption in the visible range after a UV-induced reaction [50], suggesting the formation of intermediate active species.

4.3. Comparison between the photocatalytic systems

As the results suggest, the photocatalytic efficiency is dependent on the nature of the redox reaction involved

in the process, which is a common fact in heterogeneous photocatalysis.

It has been proposed that the photocatalytic oxidation of nitrite is a fast process of $HO^{\bullet}$ attack, that may take place probably at the interface [31]. Therefore, surface properties, as the affinity of the substrate for the surface, have in this reaction a determining role. The influence of this factor is reflected in the variation of NO_2^- adsorption with the increase of the Fe content (see Table 2) and affects notably the reaction rate. For example, comparing 0–500 and 5–500 at pH 4, while the adsorption degree is doubled, the photonic efficiency triplicates in the doped sample.

This effect is less marked in the slower reactions, i.e., the oxidation of EDTA and the Cr(VI) reduction. The relative differences in adsorption between the pure and the doped samples are not large, and the same trend is observed in the reaction rates.

According to the results of characterization of the samples, in the ZrO_2-based catalysts containing up to 5% Fe, iron is not preferentially located at the surface, suggesting the formation of an external layer of zirconia [36,37]. In the case of the samples containing a higher Fe content, iron oxide is not segregated at the surface and a solid solution is observed [38]. In any case, there is no Fe excess in the surface in any sample. However, the presence of iron could modify the surface properties of the material regarding the type of active sites, presence of defects, etc., which could increase the adsorption and favor the interfacial reactions. In slower reactions, it is probable that the influence of bulk properties on the photocatalytic rate overcome that of surface properties.

The case of the complex Cr(VI)/EDTA system is different, because electron transfer processes in possible intermediate Cr(V)–EDTA species could trigger the reaction. This is the only system, among the ones studied here, in which iron exerts a deleterious effect on the initial rate, and should be object of a more detailed and complete study.

4.4. Stability of the photocatalysts

The results indicate that the samples synthesized by the sol–gel method do not suffer photodissolution in the irradiation conditions. Due to this advantageous property, it should be possible, in principle, their reuse.

No thermodynamic data for Zr dissolution is available in the literature [51], and we assume that photodissolution is not possible in these conditions. Concerning Fe dissolution, as previously mentioned, IEP and XPS data suggest that there is no Fe(III) excess on the surface and, in consequence, the particles would be more resistant to Fe photocorrosion.

However, the lack of dissolved Zr and Fe detection only indicates the absence of photodissolution but it does not eliminate the possibility of photocorrosion without dissolution, due to surface transformation. Only kinetic experiments carried out with reused samples are adequate to demonstrate the stability of the photocatalysts. Experiments in this sense are in progress.

4.5. Comparison with other photocatalysts

Although the calculated bandgap energies of the ZrO_2 samples prepared by the sol–gel technique are close to that of P-25 (3.1 eV [52]), the photocatalytic efficiencies of both types of photocatalysts in the range of wavelengths used in this work are significantly different.

It must be noticed that, to warrant a total incident light absorption, a 4-fold amount of ZrO_2-based catalysts is needed in comparison to P-25. The higher activity of P-25 could be assigned to a higher efficiency in the separation of the photogenerated charges (less e^-/h^+ recombination rate) due to the special structure of this material [52]. On the other hand, ZrO_2 samples present a very low absorbance in the near UV range that can be attributed to intrabandgap surface states. Therefore, the low activity of ZrO_2 samples can arise from the contribution of these surface states. The new samples, as well as the commercial Degussa ZrO_2, present, in contrast, intense absorption bands in the short UV range, around 230 nm [36–38]. It would be interesting, then, the comparison of the photoactivity of the samples with that of P-25 under short UV irradiation. Experiments in this direction are underway. Also, differences in back-scattering between the ZrO_2 and TiO_2 samples, which originate important losses in the absorbed light, can account for differences in the activity. Other favorable factors of P-25 are the somewhat higher specific surface area ($49\ m^2\ g^{-1}$), a smaller particle size and a lower amount of defects in the structure. Nevertheless, important advantages of the new Fe–ZrO_2 samples compared with Fe-doped titania are the enhancement of the activity compared with the pure specimens, the absence of photodissolution after illumination [26,29–32,34] and the higher particle size that facilitates their recovery from the reaction medium by fast precipitation.

5. Conclusions

The photocatalytic activity in the near UV range of zirconia and Fe/zirconia samples prepared by a sol–gel technique was tested in systems of environmental interest. All samples were found active, although its efficiency was lower compared to that of TiO_2 P-25. The incorporation of Fe(III), acting as an electron or hole trapping center in zirconia, improved the photocatalytic activity. This behavior was observed in the oxidations of NO_2^- and EDTA and in the reduction of Cr(VI). In contrast, in the case of the Cr(VI) reduction in the presence of EDTA, the photocatalytic efficiency decreased slightly with the iron content.

The different activities of the samples have been associated not only to differences in structural, optical and surface properties, affected by the conditions of synthesis, but also

to the nature and conditions of the photocatalytic reaction. In the case of Cr(VI) reduction in the presence of EDTA, the yield of the ZrO_2-based catalysts was similar to that of P-25. These results are promising, as photocatalysis emerges an adequate procedure for the treatment of real wastewaters, where oxidants and reductants are simultaneously present. In addition, the new zirconia samples do not suffer photocorrosion after the irradiation tests and, owing to their large particle size (see Table 1), are easily separable from the reaction medium.

The results of this work are meaningful for future studies on the improvement of the TiO_2 photocatalytic efficiency. Binary Ti/Zr oxides have been reported to present an enhanced photocatalytic performance [53]. Further complementary investigations with ternary Fe/Zr/Ti oxides are needed to test the photocatalytic activity of these materials and are in progress.

Acknowledgements

Work performed as part of Comisión Nacional de Energía Atómica CNEA-CAC-UAQ project #95-Q-03-05. J.A.N. thanks "Dirección General de Investigación Científica y Técnica (DGICYT-Spain), PB96-1346" for supporting part of this work. S.G.B. thanks CNEA for a fellowship to perform this work. M.I.L. wish to thank Fundación Antorchas (Argentina) a grant for travel expenses to Sevilla. M.I.L. is a member from CONICET (Argentina).

References

[1] D.A. Ward, E.I. Ko, Chem. Mater. 956 (1993).
[2] H.H. Kung, Transition Metal Oxides. Surface Chemistry and Catalysis, Studies Surface Sci. Catal. 45 (1989).
[3] A. Corma, Chem. Rev. 95 (1995) 559.
[4] J.G. Bendoraitis, R.E. Salomon, J. Phys. Chem. 69 (1965) 3666.
[5] P. Clechet, J.-R. Martin, R. Ollier, C. Valloy, C.R. Acad. Sci. Paris 282 Série C (1976) 887.
[6] J.-M. Herrman, J. Disdier, P. Pichat, J. Chem. Soc. Faraday Trans. 1 (1981) 77.
[7] A.R. Newmark, U. Stimming, Langmuir 3 (1987) 905.
[8] S. Preusser, U. Stimming, K. Wippermann, Electrochim. Acta 39 (1994) 1273.
[9] S. Sato, T. Kadowaki, J. Catal. 106 (1987) 295.
[10] H. Wiemhöfer, U. Voher, Ber. Bunsenges Phys. Chem. 96 (1992) 1646.
[11] K. Ganguly, S. Sarkar, S. Bhattacharyya, J. Chem. Soc. Chem. Comm. (1993) 683.
[12] J.A. Navío, G. Colón, Stud. Surf. Sci. Catal. 82 (1994) 721.
[13] K. Sayama, H. Arakawa, J. Phys. Chem. 97 (1993) 531.
[14] K. Sayama, H. Arakawa, J. Photochem. Photobiol. A: Chem. 94 (1996) 67.
[15] J.A. Navío, G. Colón, J.-M. Herrmann, J. Photochem. Photobiol. A: Chem. 108 (1997) 179.
[16] P. Pichat, J.-M. Herrmann, J. Disdier, M.-N. Mozzanega, J. Phys. Chem. 83 (1979) 3122.
[17] G. AlSayyed, J.C. D'Oliveira, P. Pichat, J. Photochem. Photobiol. A: Chem. 58 (1991) 99.
[18] J.A. Navío, G. Colón, M. Macías, P.J. Sánchez-Soto, V. Augugliaro, L. Palmisano, J. Molec. Cat. A: Chem. 109 (1996) 239.
[19] M.A. Fox, H. Ogawa, P. Pichat, J. Org. Chem. 54 (1989) 3847.
[20] F. Juillet, F. Lecomte, H. Mozzanega, S.J. Teichner, A. Thevenet, P. Vergnon, Faraday Symp. Chem. Soc. 7 (1973) 57.
[21] H. Courbon, P. Pichat, C.R. Acad. Sci. Paris 285 Série C (1977) 171.
[22] Y. Kohno, T. Tanaka, T. Funabiki, S. Yoshida, Chem. Commun. (1997) 841.
[23] Y. Kohno, T. Tanaka, T. Funabiki, S. Yoshida, J. Chem. Soc. Faraday Trans. 94 (1998) 1875.
[24] Y. Kohno, T. Tanaka, T. Funabiki, S. Yoshida, Chem. Lett. (1997) 993.
[25] M.A. Fox, M.T. Dulay, Chem. Rev. 93 (1993) 341.
[26] M.I. Litter, J.A. Navío, J. Photochem. Photobiol. A: Chem. 98 (1996) 171.
[27] J.A. Navío, M. Macías, M. González-Catalán, A. Justo, J. Mater. Sci. 27 (1992) 3036.
[28] A. Milis, I. Peral, X. Domènech, J.A. Navío, J. Molec. Catal. 87 (1994) 67.
[29] M.I. Litter, J.A. Navío, J. Photochem. Photobiol. A: Chem. 84 (1994) 183.
[30] J.A. Navío, G. Colón, M.I. Litter, G.N. Bianco, J. Molec. Catal. 106 (1996) 267.
[31] J.A. Navío, G. Colón, M. Trillas, J. Peral, X. Domènech, J.J. Testa, D. Rodriguez, J.R. Padrón, M.I. Litter, Appl. Catal. B: Environ. 16 (1998) 187.
[32] E.A. San Román, J.A. Navío, M.I. Litter, J. Adv. Oxid. Technol. 3 (1998) 261.
[33] J.A. Navío, G. Colón, M. Macías, C. Real, M.I. Litter, AppI. Catal. A: General 177 (1998) 111.
[34] J.A. Navío, J.J. Testa, P. Djedjeian, J.R. Padrón, D. Rodríguez, M.I. Litter, Appl. Catal. A: General 178 (1999) 191.
[35] M.I. Litter, Appl. Catal. B: Environ., in press.
[36] S. Botta, Master Thesis, Universidad de General San Martín, Buenos Aires, 1998.
[37] J.A. Navío, M. Macías, P.J. Sánchez-Soto, M.C. Hidalgo, G.M. Restrepo, S. Botta, M. Litter, M.V. Tsodikov, Actas del XVI Simposio Iberoamericano de Catálisis, A. Centeno, SA. Giraldo, E.A. Páez Mozo (Eds.), Vol. III, Cartagena de Indias, 1998, pp. 1829–1834.
[38] J.A. Navío, M. Macías, P.J. Sánchez-Soto, M.C. Hidalgo, G.M. Restrepo, S. Botta, M. Litter, M.V. Tsodikov, submitted for publication.
[39] C.G. Hatchard, C.A. Parker, Proc. R. Soc. A 235 (1956) 518.
[40] Colorimetric Determination of Non Metals, D.F. Boltz (Ed.), Interscience, New York, 1958, p. 124.
[41] K.L.E. Kaiser, Water Res. 7 (1973) 1465.
[42] C. Wei, S. German, S. Basak, K. Rajeshwar, J. Electrochem. Soc. 140 (1993) L60.
[43] Colorimetric Determination of Traces of Metals, EB. Sandell (Ed.), 2nd ed., Interscience Publishers, New York, 1950, pp. 638–642.
[44] D.L. Leussing, I.M. Kolthoff, J. Am. Chem. Soc. 75 (1953) 390.
[45] M.C. González, A.M. Braun, Res. Chem. Intermed. 21 (1995) 837.
[46] M.R. Hoffmann, S.T. Martin, W. Choi, D. Bahnemann, Chem. Rev. 95 (1995) 69.
[47] M. Tsodikov, O. Bukhtenko, O. Ellert, V. Shcherbakov, D. Kochubey, J. Mater. Sci. 30 (1995) 1087.
[48] M. Beck, D. Durham, J. Inorg. Chem. 33 (1971) 461.
[49] K.A. Easom, R. Bose, Inorg. Chem. 27 (1988) 2331.
[50] H. Fu, G. Lu, S. Li, J. Photochem. Photobiol. A: Chem. 114 (1998) 81.
[51] D. Tuck, Standard Potencials in Aqueous Solution, A. Bard, R. Pearson, J. Jordan (Eds.), IUPAC, New York, 1985, pp. 547–552.
[52] R.I. Bickley, T. González-Carreño, J.S. Lees, L. Palmisano, R.J.D. Tilley, J. Solid State Chem. 92 (1991) 178.
[53] X. Fu, L.A. Clark, Q. Yang, M.A. Anderson, Environ. Sci. Technol. 30 (1996) 647.